Cascaded Multilevel Inverter Based Power and Signal Multiplex Transmission for Electric Vehicles

Yixuan Zhang, Guipeng Chen, *Member, IEEE,* Yihua Hu, *Senior Member, IEEE*, Chao Gong, and Yangang Wang, *Senior Member, IEEE*

***Abstract*—Power & signal multiplex transmission (P&SMT) is a technique that uses power electronic circuits for communication signal transmission. In this paper, a three-phase cascaded multilevel inverter-based P&S MT system is proposed. The proposed method can transmit communication signals without using a Controller Area Network bus, thereby reducing the wiring cost of the conventional electric vehicle (EV) communication system. The designed system can achieve motor speed regulation and battery balance discharging for EVs. With the combined pulse width modulation scheme and frequency shift keying method, both power and communication signals are transmitted successfully in a simulation model implemented in Matlab/Simulink. By evaluating the bit error rate of the transmitted signal, the maximum signal rate of the proposed system is determined as 600 bit/s.**

***Index Terms*—Battery state of charge, controller area network, frequency shift keying, motor speed control, pulse width modulation, three-phase DC-AC converter.**

I. Introduction

THE challenges posed by climate change are spurring experts and researchers to investigate the alternatives for fossil fuels to achieve carbon dioxide emissions reduction. Nowadays, the application of electric vehicles provides a feasible solution for energy saving and emission reduction in the automotive industry. Compared to the traditional internal combustion engine cars, electric vehicles (EVs) not only produce fewer air pollutants such as CO and NO_x, but also generate less noise [1], [2]. Furthermore, if the battery of EV is charged at night, it can avoid the peak of power consumption, which is beneficial to the grid to balance the load and reduce the cost [3]. Since various subsystems such as the motor control unit (MCU) and the battery management system (BMS) in an EV require communication with the transmission control unit (TCU), it is necessary to employ an effective method to realize signals transmission [4], [5]. One of the approaches that is widely accepted by manufacturers and researchers for data transmission in EV is through a Controller Area Network (CAN) bus because of its high reliability and high communication baud rate [6], [7].

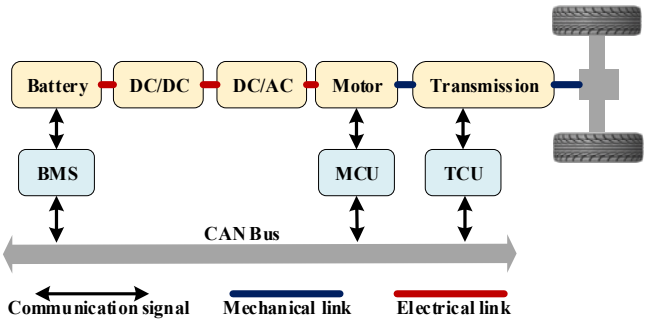

Fig. 1. The general powertrain structure of an EV

The general powertrain structure of an EV is exhibited in Fig.1. Some conventional power systems for EVs employ a DC/DC converter to boost the battery voltage for a 2-level inverter [8], [9]. This approach can have a high voltage change rates (dV/dt), which leads to high switching losses [8]. Moreover, such the system is expensive and has low power density because of the utilized bulky inductors for the DC/DC boost converters [9]. Although the traditional EVs realize their internal communication through the CAN bus, the communication channel and the power transmission line are still two independent sections, and the whole system can still be optimized.

This paper proposes a power & signal multiplex transmission (P&SMT) method to transmit both power and communication signals through a three-phase multilevel inverter circuit for EVs. The individual devices of the multilevel inverter have a much lower switching losses than that of a 2-level inverter, and a DC/DC converter is not required since the cascaded multilevel inverter itself can boost the battery voltage. In the proposed system, the power conversion is realized by the pulse width modulation (PWM) method, and the transmitted signals are modulated by the frequency shift keying (FSK) approach. Instead of using a CAN bus as a communication channel in the up-to-date EVs, the proposed approach can greatly reduce the expenditure on the communication system because the power and signals are transmitted simultaneously through the same power line.

Manuscript was submitted for review on 07, November, 2019.

Y. Zhang, Y. Hu, and C. Gong are with the Department of Electronic Engineering, University of York, York YO10 5DD, U.K. (e-mail: yz4434@york.ac.uk; yihua.hu@york.ac.uk; cg1391@york.ac.uk).

G. Chen is with the School of Aerospace Engineering, Xiamen University, Xiamen 361005, China. (E-mail: cgp2017@xmu.edu.cn).

Y. Wang is with the Dynex Semiconductor Ltd, Lincoln LN6 3LF, U.K. (e-mail: Yangang.Wang@dynexsemi.com).

Digital Object Identifier 10.30941/CESTEMS.2020.00017

The remainder of this paper is arranged as below. Section II reviews some relevant literatures about the P&SMT technique. Section III describes the structure and the P&SMT mechanisms of the proposed system. The simulation results are provided in Section IV. Section V draws a brief conclusion at the end of this paper.

II. Literature Review

There are several power and signal transmission methods that have been applied in various areas. For example, the general method for transmitting data through a power line is to modulate the data onto a high-frequency carrier, and then couple the data to the power line through a coupling circuit after power amplification [10]. Since the power line itself is not designed to transmit communication data, adding signals on it can increase the complexity of the power line channel. Additionally, the electromagnetic interference should be considered while designing a broadband power line communication (PLC) model as its 2 MHz to 32 MHz carrier frequency may coincide with the frequency of short-wave radios [11]. Power over Ethernet (PoE) is the technology that uses twisted-pair Ethernet cabling to pass data along with electric power to some IP-based terminals such as voice-over-Internet telephones and IP camera [12]. However, because the maximum output power of power sourcing equipment of PoE is larger than 15.4W in the standard IEEE802.3af, such technique is not suitable for pan–tilt–zoom camera and other high power required applications [13].

In order to expand the application range of power and signal transmission technology, literature [14] proposes the concept of power electronic signalling, which aims to use power electronic devices for communication signals generation. The generated signals can then be used for power line communication, online condition monitoring, fault detection and active protection in smart grid, distributed power generation, and other areas where simultaneous transmission of power and signals is required.

The approaches of using power electronic circuits for signal transmission are investigated in recent years. The literature [15]-[17] utilizes the Buck circuit with a multipath load structure to realize the signal transmission function while converting power. By adjusting the switching frequency with PWM technique, the switching ripple generated on the input bus can be modulated with the FSK method. In their experiments, a peak detection circuit is employed to capture the switching signal, then followed by band-pass filtering and signal processing to identify the digital '0' and '1'. The literature [18] and [19] employ a time-division multiplexing method for transmitting both communication signal and power through a DC/DC topology. In their design, signals' bidirectional transmission is realized between a master module and slave modules. Because various switches operate with different duty ratio, power and signal are transmitted alternatively through a single topology and the transmitted signals are extracted by detecting the alteration of the bus voltage. Nevertheless, such a system has a low communication rate as the signals are discontinuously transmitted.

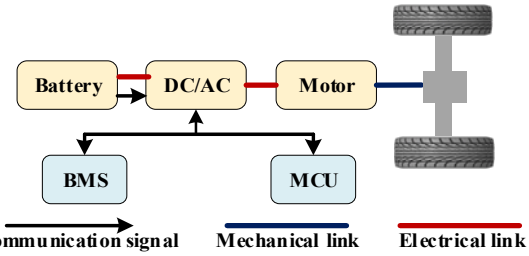

Fig. 2. The proposed system structure of an EV using the P&SMT method.

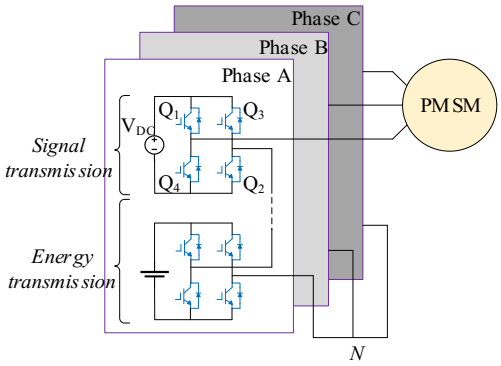

Fig. 3. Topology of the proposed P&SMT system for EVs.

III. Proposed Power and Signal Multiplex Transmission

A. System Structure

This paper elaborates the principle of the proposed P&SMT method by using the transmitted battery state of charge (SOC) signal and motor speed control signal as an example. The proposed system structure of an EV using the P&SMT method is shown in Fig. 2. The communication between the battery and BMS, and that between the MCU and motor are realized by transmitting signals through a three-phase multilevel inverter circuit. The proposed topology of a three-phase P&SMT system is indicated in Fig. 3. Specifically, each phase of the inverter topology contains four series connected H-bridge cells, where the cell powered by a DC voltage source is used for signal transmission, and the rest three cells powered by batteries are applied for energy transmission. The motor speed adjustment signal and the SOC signal are transmitted through the phase A and phase B branch respectively. In this model, a permanent magnet synchronous motor (PMSM) is applied as a load of the inverter topology.

B. Signal Transmission

The signals are modulated by the FSK method in the proposed system and the signal transmission scheme is presented in Fig. 4. If the transmitted 4-bit signal S_I is '1010', then two carriers with different frequencies shown in S_C can be applied for modulating digital '1' and digital '0' respectively. Since the signal is designed to be transmitted through an H-bridge cell in each phase, such the signal can be modulated by controlling the fast switching process of the four switches in the cell. Specifically, a switch will turn on if a digital '1' is applied as a gate signal and it will turn off when digital '0' is used. In Fig. 3, the switches Q_1 and Q_2 operate simultaneously

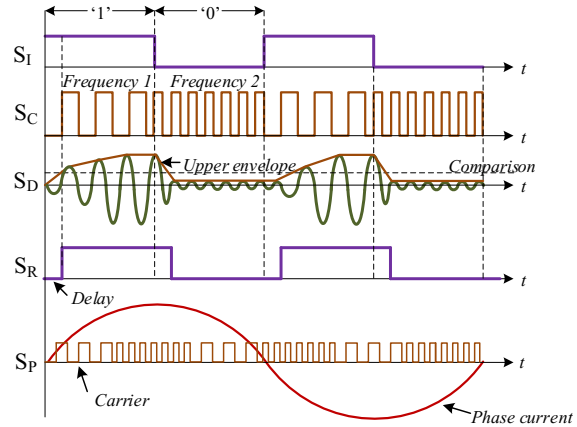

Fig. 4. The signal transmission scheme of the proposed system, where S_I is the initial 4-bit signal '1010'; S_C is the carrier waveform; S_D represents the extracted carrier for digital '1' after using a band-pass filter; S_R shows the restored signal; S_P is the output phase current waveform superimposed with the signal's carrier.

and the switches Q_3 and Q_4 turn on and turn off at the same time. Besides, the switches Q_1 and Q_2 operate with the opposite state to that of the switches Q_3 and Q_4 to avoid short circuit. Because the H-bridge cell used for signal transmission is series connected with the other three cells applied for energy transmission, the transmitted signal can be considered as superimposed on the output current waveform.

Then a band-pass filter is employed to extract the transmitted signal from the output current waveform at receiver. For any signal *f(x)* with period T and angular frequency $\omega=2\pi/T$, its Fourier series expansion can be expressed as

$$F(x)=\frac{1}{2}a_0+\sum_{n=1}^{\infty}\left(a_n\cos n\omega x+b_n\sin n\omega x\right) \tag{1}$$

where the coefficients a_0, a_n, and b_n in this series are defined by

$$\begin{cases} a_0=\dfrac{2}{T}\displaystyle\int_{-T/2}^{T/2}f(x)\,dx \\ a_n=\dfrac{2}{T}\displaystyle\int_{-T/2}^{T/2}f(x)\cos n\omega x dx \\ b_n=\dfrac{2}{T}\displaystyle\int_{-T/2}^{T/2}f(x)\sin n\omega x dx \end{cases} \tag{2}$$

Similarly, if a square wave *f(t)* with period T is applied as a carrier for digital '1', it can be expressed as

$$f(t)=\begin{cases} 0 & -\dfrac{T}{2}\le t<0 \\ 1 & 0\le t\le\dfrac{T}{2} \end{cases} \tag{3}$$

The Fourier series expansion of *f (t)* is derived as

$$F(t)=\frac{1}{2}+\frac{2}{\pi}\sin x+\frac{2}{3\pi}\sin 3x+\frac{2}{5\pi}\sin 5x+\frac{2}{7\pi}\sin 7x+\ldots +\frac{2}{n\pi}\sin nx \tag{4}$$

where n is an odd number. Because the Fourier series expansion of *f(t)* only contains the odd harmonic components, and the first-order harmonic has the largest amplitude, the first-order harmonic can be utilized for restoring the communication signals. For instance, the curve S_D in Fig. 4 represents the demodulated carrier for digital '1', then its upper envelope can be acquired using an envelope detector. With an appropriate comparison value, the upper envelope can be recovered to digital '1' when its amplitude larger than the comparison value. Otherwise, it will be recovered to digital '0'. Finally, the restored S_R is obtained after sampling the recovered digital signal using the initial bit rate of S_I.

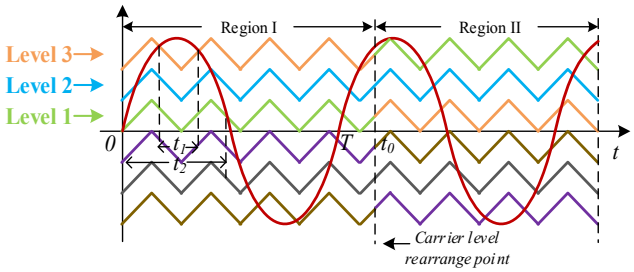

Fig. 5. Carrier level rearrangement in the PWM process.

C. Motor Speed Regulation and Battery Balance Discharging

In the proposed system, the motor speed is managed by setting the power frequency to different values with the transmitted signal. Expressly, the relationship among the motor speed n, pole-pair p, and power frequency f for a PMSM is indicated as

$$n=\frac{60f}{p} \tag{5}$$

where the constant 60 refers to 60 s/min. Theoretically, the speed of a 2-pole pair motor should change between 1200 r/min and 1800 r/min if its power frequency varies between 40 Hz and 60 Hz. With the transmitted signal s, the power frequency f is then calculated by

$$f=20\times s+40 \tag{6}$$

The power frequency will be 40 Hz and 60 Hz if the digital '0' and digital '1' occur in the transmitted signal s respectively. Next, the three-phase reference sinusoidal waves are obtained from

$$\begin{cases} P_a=A\sin(2\pi f) \\ P_b=A\sin\left(2\pi f-\dfrac{2}{3}\pi\right) \\ P_c=A\sin\left(2\pi f-\dfrac{4}{3}\pi\right) \end{cases} \tag{7}$$

where P_a, P_b, and P_c represent the reference wave in phase A, phase B, and phase C respectively, and A is amplitude. The phase B and phase C reference waves lag the phase A reference wave by $2\pi/3$ and $4\pi/3$ radians respectively. Finally, the modulated variable frequency sine waves are used to drive the motor to achieve motor speed adjustment.

In the conventional sinusoidal PWM method, the gating signal of a switch is generated by comparing the reference wave with a triangular carrier. Because various carriers and the reference wave intersect at different positions, the duty cycle of each switch is different. For instance, in a single period from 0 to T as displayed in Fig. 5, the duty cycle of a switch controlled by 'Level 3' carrier is smaller than that of the other switch modulated by 'Level 1' carrier ($t_1<t_2$). Since the input power

TABLE I
PARAMETERS VALUE USED IN THE PROPOSED SYSTEM

Parameter name	Value
DC voltage source	30 V
Battery voltage	48 V
PWM carrier frequency	2 kHz
PWM referenced sine wave frequency	40 Hz, 60 Hz
Carrier frequency of motor speed adjustment signal	4 kHz for '1' and 8 kHz for '0'
Carrier frequency of SOC signal	6 kHz for '1' and 10 kHz for '0'

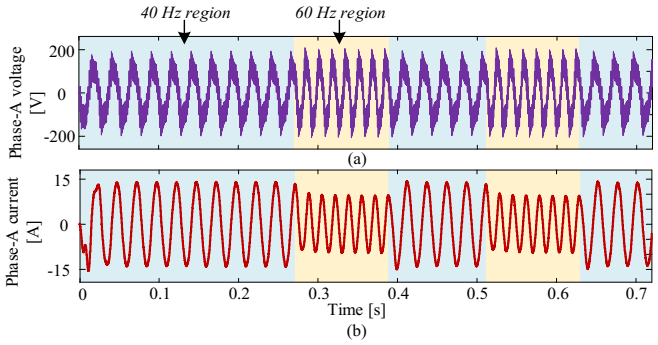

Fig. 6. (a) The output voltage waveform of phase A and (b) the output current waveform of phase A

comes from batteries, the switch operating with a smaller duty cycle consumes less power than the switch operating with a larger duty cycle. This will further lead to the case of batteries' remaining capacity being unbalanced after the system running for a while. Therefore, the battery balance discharging can be realised by periodically rearranging the carrier levels within the PWM process. To achieve this target, firstly, the battery SOC values at the periodical sampling point are combined to form a data stream and transmitted through the DC voltage source powered full-bridge cell using FSK method. After demodulating the signal from the phase current, the SOC values are separated into different decimal numbers. Finally, the carrier levels of PWM are rearranged according to the transmitted SOC values (at t_0 in Fig. 5 for example), and the battery balance discharging is realized.

IV. SIMULATION RESULTS AND ANALYSIS

A. Simulation Parameters and Output Waveforms

Based on the mechanisms demonstrated in section III, a simulation model is built in Matlab/Simulink. Table I summarises the values of parameters in the simulation model. Each H-bridge cell for power transmission contains a 48 V battery, and a 30 V DC voltage source is applied in each H-bridge circuit for signal transmission. Therefore, the amplitude of the transmitted signal is neither too small to be restored, nor too large to seriously affect the output sinusoidal waveform. Moreover, because the system employs the carriers with the frequency distribution from 2 kHz to 10 kHz, it is appropriate for silicon type IGBT devices to operate in such a frequency range [20].

When connecting a PMSM as a load to the output side of the three-phase inverter circuit, the output voltage and current waveforms measured by a voltage sensor and a current sensor

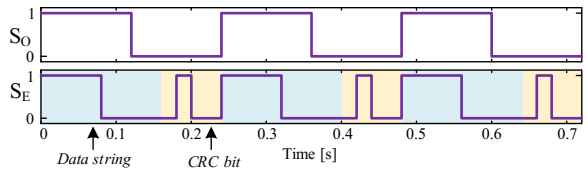

Fig. 7. S_O represents for the original 8-bit data string and S_E refers to the entire 12-bit transmitted signal.

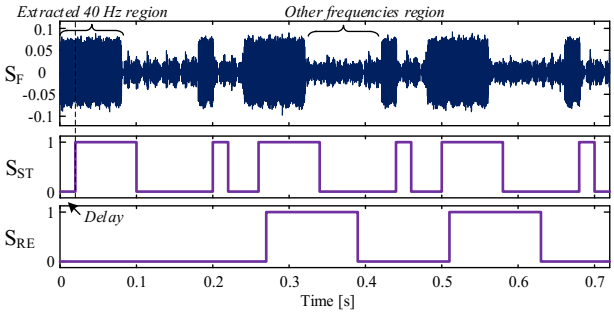

Fig. 8. S_F represents the extracted 4 kHz carrier after the filtering process; S_{ST} is the recovered 12-bit signal; S_{RE} is the restored 8-bit motor speed adjustment signal.

are exhibited in Fig. 6. Since there are three batteries and a DC voltage source in each phase, the maximum phase voltage is 174 V (3×48+30=174). It can be observed that the amplitude of the phase current waveform varies at around 0.27 s and 0.51 s, and this is because the motor power frequency changes from 40 Hz to 60 Hz at these time points.

B. Motor Speed Adjustment Signal Transmission

An original 8-bit motor speed adjustment signal is set as 11110000 with 0.03 s per bit, thus the signal transmitting rate is 100/3 bps. Then a 4-bit cyclic redundancy code (CRC) is added at the end of each 8-bit data string to separate two adjacent data strings. Because the generated 4-bit CRC code is 0100 by using the generator polynomial $x^4 + x^3 + x^2 + x + 1$, the entire 12-bit data frame is 111100000100. Dividing the transmitted data frame by the modulo-2 division approach with the divisor 11110, the system can determine whether the frame data is erroneous by verifying whether the remainder is zero. If it is 0, it proves that the frame data has no errors during the transmission, otherwise an error occurs. Both the original message data and the message data followed by the CRC code is shown in Fig. 7. It is worth mentioning that the time used for transmitting a frame with a CRC code and without a CRC code are the same, thus the 12-bit data is transmitted with 0.02 s per bit. After the entire data frame is obtained, the 4 kHz square wave is applied as a carrier for digital '1' and the 8 kHz square wave is used as a carrier for digital '0'.

Next, the signal is transmitted through an H-bridge cell, and the 4 kHz carrier is extracted from the phase current waveform with a band-pass filter. Then the filtered carrier waveform S_F in Fig. 8 is used to recover the transmitted signal with an appropriate threshold value. Since the attenuation at cut-off frequencies is fixed at 6 dB in this band-pass filter, the attenuation ratio x can be calculated as 0.5 from

$$20 \log x = -6 \tag{8}$$

In other words, the amplitude of waveform S_F in cut-off

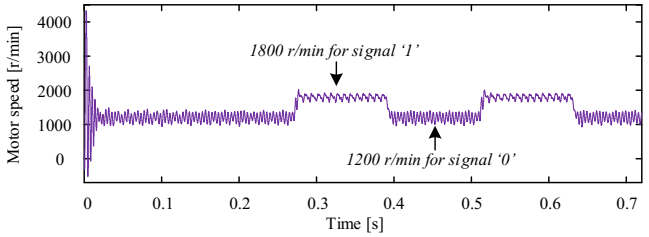

Fig. 9. The controlled motor speed with the transmitted 8-bit signal '11110000'.

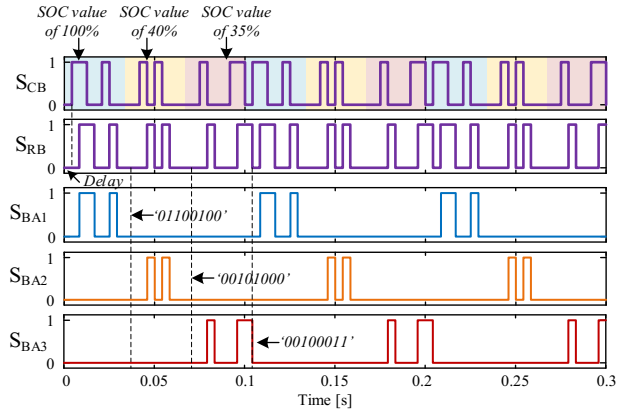

Fig. 10. S_{CB} is the code string formed by the three SOC frames; S_{RB} is the recovered SOC signal; S_{BA1} contains the frame '01100100', which indicates the SOC of the first battery; the frame '00101000' in S_{BA2} refers to the SOC of the second battery; the frame '00100011' in S_{BA3} represents the SOC of the third battery.

frequencies region (0.04) is half of its amplitude in the passband frequencies region (0.08). Therefore, '0.05' is selected to separate the cut-off frequencies region and passband frequencies region of the filtered wave. When collating the recovered signal S_{ST} in Fig. 8 with the waveform S_E in Fig. 7, it can be observed that there exists a delay in S_{ST}, which is mainly caused by the filtering process. After removing the 4-bit CRC code after each 8-bit data frame, the restored signal S_{RE} in Fig. 8 is obtained. Because the 4-bit CRC code first occurs at 0.18 s (0.02×8+0.02(one-bit delay)=0.18), the transmitted data before the CRC code in the first period is 'ignored' by the system. Additionally, the recovered data frame has the same rate (0.03 s per bit) as its original signal rate. Therefore, the restored 8-bit data frame first appears at 0.27 s (0.03×8+0.03(one-bit delay)=0.27), and S_{RE} can be considered as delaying a whole signal period plus one sampling time.

Finally, the recovered signal S_{RE} in Fig. 8 is utilized to manage the motor speed, whose waveform is displayed in Fig. 9. Whenever the signal changes between '0' and '1', the motor speed fluctuates for about 0.01 s. Since the power frequency is designed to alternate between 40 Hz and 60 Hz, the motor speed stabilizes at 1200 r/min and 1800 r/min as expected. Because the transmitted signal is superposed on the phase current in the form of energy, the transmitted signal will interfere with the phase current waveform, thus affecting the stability of motor speed. Additionally, as the motor speed is open-loop controlled by adjusting the motor power frequency, its steady-state fluctuation is larger than the conventional double closed-loop control approach.

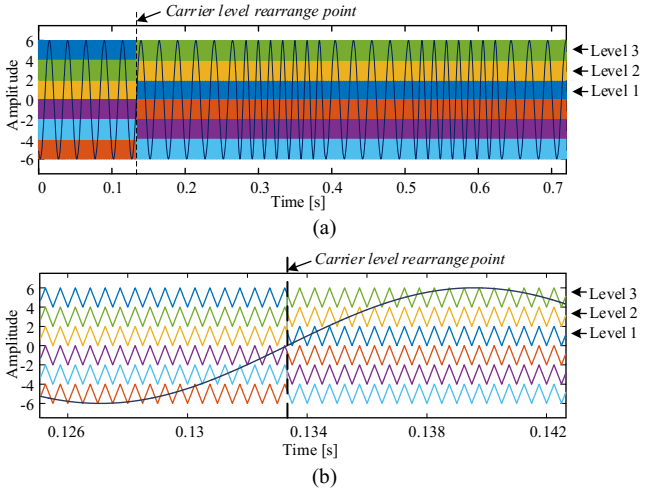

Fig. 11. The rearranged carriers and the reference sinusoidal wave used in the PWM process, where (a) is the original image, and (b) is the enlarged image at the carrier level rearrange point.

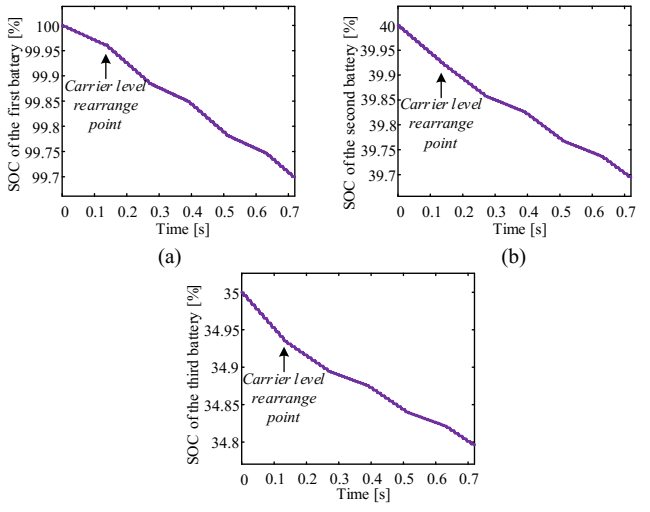

Fig. 12. The SOC curves of the three batteries, where (a), (b), and (c) refer to the battery with the initial SOC of 100%, 40%, and 35% respectively.

C. SOC Signal Transmission

The three phase-B batteries' SOC values are transmitted through its phase current in this simulation. Firstly, the initial SOC values of the three batteries are set as 100%, 40%, and 35% respectively, thus the transmitted three frames are '01100100', '00101000', and '00100011' in binary format. Then the three binary strings are combined to form a new code string S_{CB} as displayed in Fig. 10. Since the SOC value of each battery is sampled every 0.1 s, the period of the generated code string is also set to 0.1 s to maintain the time consistent with the SOC sampling time. Therefore, the system is designed to transmit 24 bits of data every 0.1 s, and the signal rate is 240 bps. Because it usually takes a while for the SOC of the battery to change significantly, the sampled SOC values in the subsequent periods are still the same as those of the first cycle.

After demodulating the SOC signal from the phase current waveform, the recovered SOC signal S_{RB} in Fig. 10 is obtained. S_{RB} delays the original transmitted signal S_{CB} for 1-bit time (0.1/24 s), which is caused by the filtering process. S_{BA1}, S_{BA2},

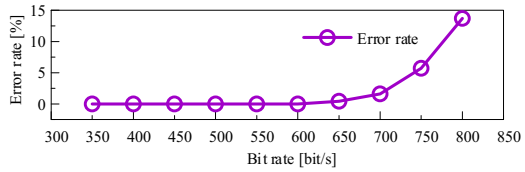

Fig. 13. The relationship between the signal bit rate and error rate.

and S_{BA3} in Fig. 10 shows the separated three SOC values from the code string S_{RB}.

Finally, the carrier levels in the PWM process are reordered for next cycle after comparing the three SOC values. Fig. 11 shows the results after the carrier levels rearranging process, from which it can be observed that the carrier levels are rearranged at 0.4/3 s. Specifically, the initial carrier levels for the H-bridge cells with the batteries SOC value of 100%, 40%, and 35% are set to level 3, level 1, and level 2 respectively, and they are repositioned to level 1, level 2, and level 3 according to the numerical sizes of the three SOC values. The carrier levels are reorganized every 0.1 s after the first rearranging point. However, the carrier levels are not changed at the subsequent level reset point in Fig. 11, which is caused by the batteries' SOC do not vary too much in a short period.

The SOC curves of the three batteries employed in phase B are presented in Fig. 12. It can be investigated that the power consumption of the motor is different when the motor is operating at different speeds. For instance, the slope of the SOC curve changes due to variation of the frequency of the modulated sine wave at 0.27 s. Furthermore, the slopes of these three curves are also altering at 0.4/3 s. At this point, the speed of the motor does not change, so the slope variation is caused by the method of reallocating the carrier levels. Specifically, the SOC of the first battery (Fig. 12(a)) suddenly decreases dramatically at 0.4/3 s as it has the largest SOC value. In addition, the decrease rate of the third battery's SOC curve (Fig. 12(c)) becomes the slowest at the same time since it has the smallest SOC value. The simulation results prove that the battery balance discharging is achieved successfully in this system.

D. System Data Transmission Capability

The maximum data transmission rate of the proposed system can be determined by calculating the error rate of the transmitted signal. When comparing the original data string and the received one bit by bit, the error rate of the transmitted signal is obtained. After gradually increasing the rate of the motor speed control signal, the relationship between the bit rate and the error rate is exhibited in Fig. 13. From this figure, the error rate starts rising when the signal rate is larger than 600 bit/s. Since the proposed system manages the batteries' discharge process according to the batteries' SOC value, there is an extremely high requirement for the correctness of the transmitted data. Once the demodulated data is incorrect, the batteries SOC sequencing does not achieve the expected results. The data rate of this system is relatively low when comparing to the conventional communication channels such as optical fibre. However, such a low data rate is acceptable in this system as the batteries' SOC value does not change significantly in a short time. Moreover, because the motor speed takes a while to stabilize after the frequency changes at each time, it is sufficient to transmit the motor speed control signal at a data rate of 600 bit/s.

V. CONCLUSION

In this paper, a three-phase multilevel inverter-based P&SMT system is proposed to achieve motor speed adjustment and battery balance discharging for EVs. Four series-connected H-bridge cells are involved in each phase of the inverter topology, where the PWM controlled three cells are used for energy transmission and the rest FSK controlled cell is applied for communication signal transmission. Since the proposed approach employs a part of the power electronic circuit as a communication channel, the complexity of the entire system can be reduced by simplifying the system wiring. With a simulation model implemented in Matlab/Simulink, the feasibility of the proposed P&SMT method is verified by transmitting the motor speed adjustment signal and the battery SOC signal through phase-A and phase-B currents respectively. Additionally, the signal transmission capability of the proposed method is determined as 600 bit/s after investigating the relationship between the signal bit rate and error rate.

REFERENCES

[1] T. Donateo, F. Licci, A. D'Elia, G. Colangelo, D. Laforgia and F. Ciancarelli, "Evaluation of emissions of CO2 and air pollutants from electric vehicles in italian cities," *Applied Energy*, vol. 157, pp. 675-687, Nov. 2015.

[2] C. Ma, C. Chen, Q. Liu, H. Gao, Q. Li, H. Gao and Y. Shen, "Sound quality evaluation of the interior noise of pure electric vehicle based on neural network model," *IEEE Transactions on Industrial Electronics*, vol. 64, no. 12, pp. 9442-9450, 2017.

[3] M. Yilmaz and P. T. Krein, "Review of the impact of vehicle-to-grid technologies on distribution systems and utility interfaces," *IEEE Transactions on Power Electronics*, vol. 28, no. 12, pp. 5673-5689, 2013.

[4] K.Ç. Bayindir, M.A. Gözüküçük and A. Teke, "A comprehensive overview of hybrid electric vehicle: Powertrain configurations, powertrain control techniques and electronic control units," *Energy conversion and Management*, vol. 52, no. 2, pp. 1305-1313, 2011.

[5] X. Zhu, H. Zhang, J. Xi, J. Wang and Z. Fang, "Optimal speed synchronization control for clutchless AMT systems in electric vehicles with preview actions," *2014 American Control Conference*, pp. 4611-4616, 2014.

[6] F. Zhou, S. Li and X. Hou, "Development method of simulation and test system for vehicle body CAN bus based on CANoe," *2008 7th World Congress on Intelligent Control and Automation*, pp. 7515-7519, 2008.

[7] M. Zheng, B. Qi and H. Wu, "A li-ion battery management system based on CAN-bus for electric vehicle," *2008 3rd IEEE Conference on Industrial Electronics and Applications*, pp. 1180-1184, 2008.

[8] L. M. Tolbert, F. Z. Peng and T. G. Habetler, "Multilevel inverters for electric vehicle applications," *Power Electronics in Transportation (Cat. No.98TH8349)*, pp. 79-84, 1998.

[9] Z. Du, B. Ozpineci, L. M. Tolbert and J. N. Chiasson, "DC–AC cascaded H-bridge multilevel boost inverter with no inductors for Electric/Hybrid electric vehicle applications," *IEEE Transactions on Industry Applications*, vol. 45, no. 3, pp. 963-970, 2009.

[10] L. Lampe, A.M. Tonello and T.G. Swart, *Power Line Communications: Principles, Standards and Applications from multimedia to smart grid*, John Wiley & Sons, 2016.

[11] W. Huagang, T. R. Meng and L. S. Wen, "Measurement and analysis of electromagnetic emissions for broadband power line (BPL) communication," *2017 IEEE 5th International Symposium on*

Electromagnetic Compatibility (EMC-Beijing), pp. 1-4, 2017.

[12] R. V. White, "Electrical isolation requirements in power-over-ethernet (PoE) power sourcing equipment (PSE)," *Twenty-First Annual IEEE Applied Power Electronics Conference and Exposition, 2006. APEC '06*, pp. 4, 2006.

[13] J. Herbold, "Navigating the IEEE 802.3af standard for PoE," *POWER ELECTRONICS TECHNOLOGY*, vol.30, no. 6, pp. 45-48, 2004.

[14] W. Xu and W. Wang, "Power electronic signaling Technology—A new class of power electronics applications," *IEEE Transactions on Smart Grid*, vol. 1, no. 3, pp. 332-339, 2010.

[15] S. Saggini, W. Stefanutti, P. Mattavelli, G. Garcea and M. Ghioni, "Power line communication in dc-dc converters using switching frequency modulation," *Twenty-First Annual IEEE Applied Power Electronics Conference and Exposition, 2006. APEC '06*, 2006.

[16] W. Stefanutti, P. Mattavelli, S. Saggini and L. Panseri, "Communication on power lines using frequency and duty-cycle modulation in digitally controlled dc-dc converters," *IECON 2006 - 32nd Annual Conference on IEEE Industrial Electronics*, pp. 2144-2149, 2006.

[17] W. Stefanutti, S. Saggini, P. Mattavelli and M. Ghioni, "Power line communication in digitally controlled DC–DC converters using switching frequency modulation,"*IEEE Transactions on Industrial Electronics*, vol. 55, no. 4, pp. 1509-1518, 2008.

[18] J. Wu, C. Li and X. He, "A novel power line communication technique based on power electronics circuit topology," *2010 Twenty-Fifth Annual IEEE Applied Power Electronics Conference and Exposition (APEC)*, pp. 681-685, 2010.

[19] J. Wu, S. Zong and X. He, "Power/signal time division multiplexing technique based on power electronic circuits," *2011 Twenty-Sixth Annual IEEE Applied Power Electronics Conference and Exposition (APEC)*, pp. 1710-1714, 2011.

[20] C. Blake and C. Bull, "IGBT or MOSFET: Choose wisely," *International Rectifier,* 2001.

Yixuan Zhang was born in Shaanxi province in P.R. China on September 1994. He received the B.Eng. and the M.Eng degree in electrical engineering from the University of Liverpool, Liverpool, UK, in 2017 and 2018, respectively. Currently, he is a Ph.D. student in the University of York.

His research interests include power & signal multiplex transmission and topology derivation of power electronics converters.

Guipeng Chen (M'18) received the B.E.E. degree in electrical engineering from Zhejiang University, Hangzhou, China, in 2011, and the Ph.D. degree in power electronics and electric drives from the College of Electrical Engineering, Zhejiang University, in 2017. During the PHD study, he joined Fuji Electric Matsumoto Factory as a summer intern in 2014 and was invited to the University of Liverpool as a research assistant for a half-year program from July 2016. He is currently working as a Postdoc at the Instrument Science and Technology Postdoc Center, School of Aerospace Engineering, Xiamen University, China. His current research interests include automatic topology derivation of dc-dc converters and fault-tolerant converters.

Yihua Hu (M'13-SM'15) received the B.S. degree in electrical motor drives in 2003, and the Ph.D. degree in power electronics and drives in 2011. Between 2011 and 2013, he was with the College of Electrical Engineering, Zhejiang University as a Postdoctoral Fellow. Between 2013 and 2015, he worked as a Research Associate at the power electronics and motor drive group, the University of Strathclyde. Currently, he is a Lecturer at the Department of Electronic Engineering, University of York (UoY). He has published 65 papers in IEEE Transactions journals. His research interests include renewable generation, power electronics converters & control, electric vehicle, more electric ship/aircraft, smart energy system and non-destructive test technology. He is the associate editor of IET Renewable Power Generation, IET Intelligent Transport Systems and Power Electronics and Drives.

Chao Gong was born in Shandong province in P.R. China, on February 22, 1991. He received the B.Eng. and the M.Eng degree in electrical engineering from Northwestern Polytechnical University, Xi'an, China, in 2014 and 2016, respectively. Currently, he is a Ph.D. student in the University of York.

His research interests include electrical machines design and drives, power electronics and motion control.

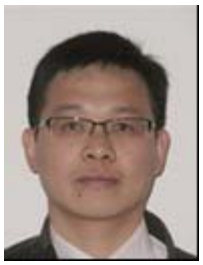

Yangang Wang (M'14-SM'16) received PhD degree in Microelectronics and Solid-State Electronics from Peking University in 2007. He joined the R&D Centre of CRRC Dynex Semiconductor Ltd in the UK as a Principal Engineer in 2012, and is currently in the leading role of the department responsible for development of advanced Si and WBG power semiconductor products.

Dr. Wang is a senior member of IEEE, member of IET and a Chartered Engineer of the UK. He has more than 20-year research and development work experience on Microelectronics and Power Electronics. His current research and development activities include design/simulation, packaging, test/characterization, failure analysis, reliability and lifetime prediction etc for power Si and WBG semiconductor devices.